Journal Name

ARTICLE TYPE

Cite this: DOI: 10.1039/xxxxxxxxxx

Aryl-Viologen Pentapeptide Self-Assembled Conductive Nanofibers†

David E. Clarke,[a‡] Magdalena Olesińska,[a‡] Tobias Mönch,[a] Ben Schoenaers,[b] Andre Stesmans,[b] and Oren A. Scherman*[a]

Received Date
Accepted Date

DOI: 10.1039/xxxxxxxxxx

www.rsc.org/journalname

Supramolecular interactions have been used to fabricate conductive nanomaterials, offering enhanced performance through 1D confined electronic properties and the ease of solution processing. We functionalized a pentapeptide motif with an asymmetric arylated methyl-viologen (AVI3D2) and utilized β-sheet self-assembly in aqueous media to drive the formation of conductive nanofibers. Through altering the concentration and pH of the solution, we demonstrated facile control over nanofiber fabrication. Using a combination of spectroscopic techniques and conductive atomic force microscopy, we investigated the molecular conformation of the resultant AVI3D2 fibers and how their conductivity is affected by β-sheet self-assembly. These conductive nanofibers have potential for future exploration as molecular wires in optoelectronic applications.

The fabrication of molecular wires and electronic circuitry is currently of great interest in nanoscience.[1] Typical approaches to generate these molecular constructs have involved the development of polymers, which can transfer charge along their extended molecular structure.[1] More recently, supramolecular interactions such as π-π stacking and the oligopeptide self-assembly of aromatic species have been used to fabricate conductive nanomaterials.[2–4] These types of constructs with nanoscale architectures have enhanced performance, taking advantage of the 1D confined electronic properties and the ease of solution processing.[2,4]

Oligopeptide β-sheet self-assembly mechanisms can generate a variety of nanostructures in aqueous solutions.[5–7] In a few examples, sequences have been able to form nanospheres,[8] fibrous and plate-like assemblies,[9] and micelles and nanotubes.[10] Through further functionalization with aromatic and hydrophobic synthetic groups,[5,11] additional π-π stacking and hydrophobic interactions can be introduced to promote self-assembly.[7] In light of this, oligopeptides have also been combined with aromatic semiconductive subunits such as perylene imide moieties in an attempt to control the assembly and enhance the semiconductivity of these subunits.[12,13] Furthermore, β-sheet assemblies formed from aromatic phenylalanine-phenylalanine dipeptide sequences have been shown to generate quantum confined structures with underlying semiconductive properties.[4,14]

Viologens (N,N'-disubstituted 4,4'-bipyridinium salts) have been of great interest in both electrochemistry and photochemistry.[15–17] They can be reduced from the dication (V^{2+}) to the radical cation ($V^{+\bullet}$) state and further to a neutral species (V^0) in two single-electron-transfer steps.[15,17] This has led to their application as redox mediators and as electron acceptors in charge-transfer complexes for electrical and ionic conductors.[15,17] Additionally, electrodes modified with viologen based polymer species have been of increasing interest due to their electric, optical and magnetic performance.[17,18] The electrochemical and spectral properties of viologen have been found to be influenced through R-group substitution at the pyridinium nitrogen atoms.[1,15,16] Where a symmetrical aryl R-group substitution coupled with additional electron donating groups has been shown to generate the largest single molecule conductance for viologen compounds.[16,19] This is thought to maximize intramolecular electron transfer across the structure, enhancing conductivity.[16,19]

We hypothesized that by functionalizing a pentapeptide motif (I3D2) with an asymmetric arylated methyl-viologen (AV), we could utilize β-sheet self-assembly in aqueous media to drive the formation of conductive nanofibers. Recently, we reported pentapeptide motifs that contain three aliphatic isoleucine (Ile) residues, an amino acid with a high propensity to form β-sheets, coupled with two aspartic acid (Asp) residues at the C-terminus which promote solubility (Figure 1a).[20] Upon protonation of the

[a] *Melville Laboratory for Polymer Synthesis, Department of Chemistry, University of Cambridge, Lensfield Road, Cambridge, CB2 1EW, UK. E-mail: oas23@cam.ac.uk*
[b] *Department of Physics and Astronomy, KU Leuven, Celestijnenlaan 200D, 3001 Leuven, Belgium*

† Electronic Supplementary Information (ESI) available: [details of any supplementary information available should be included here]. See DOI: 10.1039/b000000x/

‡ These authors contributed equally to this work.

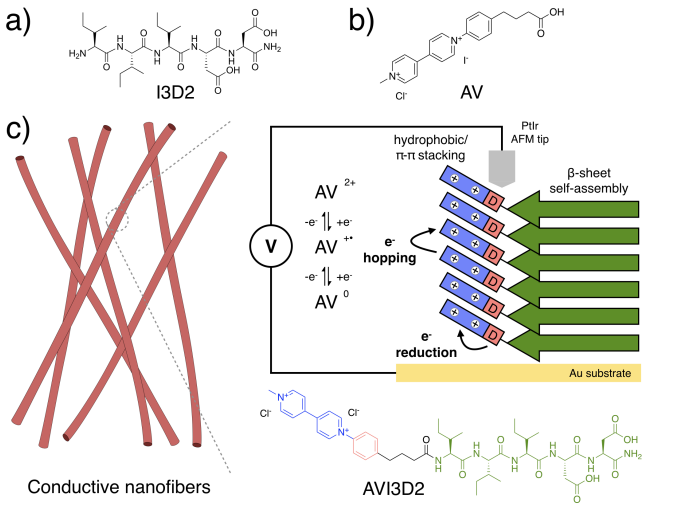

Fig. 1 Chemical structure of a) I3D2 peptide and b) AV. c) Schematic depicting the chemical structure of the AVI3D2 conjugate and the proposed supramolecular stacking arrangement of the self-assembled conductive nanofibers.

Asps, charge recognition/hydrogen bonding drives β-sheet self-assembly and in turn, the formation of nanofibers. Through simple amide coupling, we conjugated a synthesized AV molecule (Figure 1b) to the I3D2 peptide to yield an AV labelled pentapeptide sequence (AVI3D2). In this paper, we demonstrate the facile formation of conductive nanofibers in aqueous media through controlling the pH and concentration of AVI3D2 in solution (Figure 1c). Additionally, we utilize spectroscopic techniques to probe the secondary structure and molecular conformation of the resultant AVI3D2 conductive fibers to investigate how their conductivity is affected by β-sheet self-assembly.

To investigate the self-assembly of AVI3D2, stock solutions were prepared at both high (8 mM) and low (1 mM) concentrations in basic media. Small volumes of HCl were then added to achieve a final solution of pH 4, triggering the protonation of the Asp residues and consequently, the self-assembly of the peptide. Interestingly, we observed that in solution both AVI3D2 and AV have a photoluminescence (PL) with a maxima between 500-510 nm and a Stokes shift of 180-190 nm (Figures 2a, S15 and S16). The PL peak intensity and wavelength for these molecules was found to be dependent on pH. At the concentrations of 1 and 8 mM the AV molecule displayed an increase in PL in acidic conditions (Figures S15a and S15b). This phenomenon could be a product of counter ion exchange (I^- replacing Cl^-), solvation effects or through charge transfer between the carboxylic acid and aromatic part of molecule, driven by protonation induced planarisation.[21,22] At the lower concentration of 1 mM, AVI3D2 has very little change in PL at different pH with only a slight decrease in intensity observed in acidic conditions (Figure S16a). In contrast, the PL intensity of AVI3D2 (8 mM) is quenched by 40% and has a blue shift of 10 nm at pH 4 (Figure 2a). The PL of fluorescent molecules is known to be influenced by intermolecular stacking arrangements.[23] Photoinduced Electron Transfer (PET) can generate a quenching effect when donor and acceptor are in contact (on the sub-nanometer length scale) through hydrophobic and π-π stacking interactions.[23] Similarly, PET on account of the charge recombination of mixed valence viologens has been previously reported for viologen-based cyclophanes.[24,25] The interactions between the AV moeities in AVI3D2 were investigated through NOESY 2D-NMR studies, which verified the presence of intermolecular interactions (Figures S7-8, S12-13 and supplementary discussion). Therefore, both the NOESY and fluorescence spectra of AVI3D2 suggest that pH can be used to trigger the β-sheet assembly of the peptide and in turn bring the AV units into close proximity via hydrophobic/π-π stacking (Figure 1c).

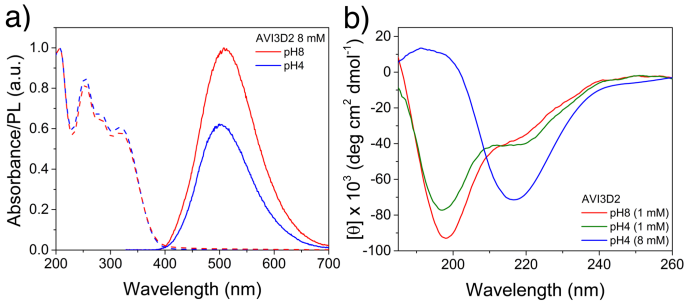

Fig. 2 a) Normalized steady-state photoluminescence spectra of AVI3D2 (8 mM) at different pH following excitation at 320 nm. Dotted lines represent absorbance of AVI3D2 (0.1 mM) at the corresponding pH. b) Circular dichroism spectra of AVI3D2 at different pH and concentrations.

To probe the supramolecular structure of the AVI3D2 molecule in its assembled state, spectroscopic techniques were utilized. In line with fluorescence spectra, CD experiments confirmed the concentration and pH dependence of the self-assembly of AVI3D2 and the I3D2 peptide (Figures 2b, S17 and S18). At a concentration of 8 mM, both AVI3D2 and the I3D2 peptide have spectra that resembles a β-sheet in acidic conditions, with a minima present at 216-220 nm (Figures 2b and S11b).[26,27] At 1 mM, both the AVI3D2 and I3D2 peptide have a CD signature of a typical random coil (Figures 2b and S11a).[27] This random coil to β-sheet transition can also be witnessed at the higher concentration of 8 mM through changes in pH. By simply altering the pH from 8 to 4, the CD spectra of both AVI3D2 and the I3D2 display a clear switch to a β-sheet signature (Figures 2b and S17b). This highlights that the protonation of the Asp residues acts as the driving force in the β-sheet formation.[20]

The CD spectra of β-sheets have a greater variability than other peptide secondary structures.[28] β-sheets have both significant intermolecular and intrastrand hydrogen bonding, and can form antiparallel, parallel, or mixed β-sheets.[27,28] Interestingly, AVI3D2 and I3D2 have distinctly different β-sheet CD signals, with I3D2 having a 4 nm red-shift in minima (220 nm) when compared to AVI3D2 (216 nm) (Figure S18b). Previous studies have suggested that a red-shift in the CD spectra of β-sheets is representative of more twisted and distorted arrangements.[20,26,28] In light of this, we can suggest that the conjugation of the AV moiety at the N-terminus of the I3D2 peptide influences the β-sheet conformation and generates less twisted stacking arrangements, likely through additional hydrophobic/π-π interactions.

This observation was further supported by the FTIR spectra of the amide I region (Figure S19), where AVI3D2 and I3D2 at 8 mM

display a prominent peak at ≈1630 cm^{-1} indicating a β-sheet conformation.[29] Recently, it has been reported that Asp positioning can influence the stacking orientation of tripeptide β-sheet structures, where Asp at the C-terminus was shown to generate a parallel β-sheet conformation.[30] Whilst it cannot be explicitly defined whether the AVI3D2 and I3D2 assemblies are in an antiparallel or a parallel orientation, the FTIR spectra for these sequences have no obvious antiparallel behavior, which is usually depicted by an amide I splitting between 1680-1690 cm^{-1}.[29] Therefore, from the combination of fluorescence, NOESY and spectroscopic studies we can suggest that both sequences form parallel β-sheets, where the planar AV region of the AVI3D2 sequence is stacked in close contact (Figure 1c).

The morphology and conductive properties of the self-assembled AVI3D2 structures were characterized using conductive atomic force microscopy (c-AFM) operating in contact mode coupled with an ORCA^{TM} cantilever. At the higher concentration (8 mM), where spectroscopic studies indicated β-sheet formation, both AVI3D2 and the I3D2 peptide formed nanofibers (Figures 3a and 3b). However at 1 mM, the I3D2 peptide and AVI3D2 conjugate formed amorphous aggregates, likely driven by drying effects (Figures S20a and S21a). Using the ORCA^{TM} module we probed the conductivity of the different materials, this technique allows for IV curve measurements to be taken at specific locations on the substrate. The AVI3D2 materials displayed a non-linear IV curve, typical for that of an organic semi-conductor, whereas the I3D2 fibers and aggregates had no apparent conductivity (Figures 3c, 3d and S21c). Interestingly, the IV curves indicated an enhanced conductivity in the AVI3D2 nanofibers (8 mM) when compared to the AVI3D2 amorphous aggregates (1 mM), where at -10 V the current increases from around -50 pA (Figure S20c, P1) to -4.0 nA (Figure 3d, P2). This is further supported by the short-circuit current map of the AVI3D2 nanofibers (Figure 3aii) and the points corresponding to where the IV curves were taken (Figures 3c and 3d). Thicker fibers/denser regions appear to be of a darker contrast, suggesting an increased conductivity, and this also correlates with the IV curves taken at points 1 and 2. Therefore, demonstrating that the β-sheet and supramolecular stacking present in the nanofibers offer an improved conductivity over the amorphous structures for the AVI3D2 materials.

The AVI3D2 nanofibers are fabricated by solution self-assembly, where the secondary structure is thought to be driven by a complimentary parallel β-sheet conformation of the peptide and hydrophobic/π-π stacking of the planar AV groups (Figure 1c). Viologens in their neutral or radical cation state are considered to have a higher conductivity than their dication form.[15,31] However, as a dication, charge transfer is permitted with a donor species (neutral or anionic) and consequently, conductivity is improved.[1] The viologen's aryl-group functionalization is known to improve intramolecular electron transfer. It acts as an electron donor (D) with the electron-poor viologen as an acceptor (A), generating an enhancement in single molecule conductivity.[16,19] With the application of charge or excitation, the dication viologen species will be reduced to either a radical cation or a neutral species through electron donation from the D-A pair.

To investigate our hypothesis of radical cation formation, AV

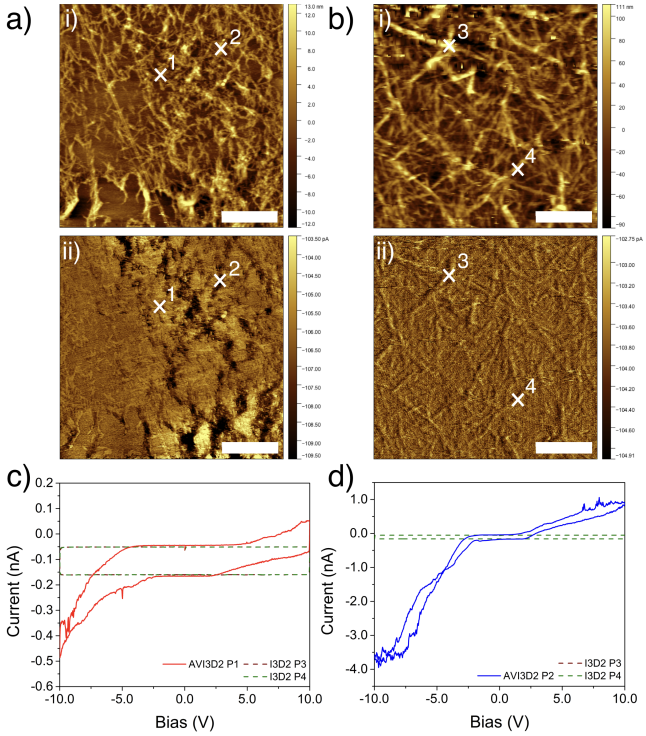

Fig. 3 c-AFM measurements of AVI3D2 and I3D2 at a concentration of 8 mM. a) Topography map (i) and short-circuit current map of AVI3D2 nanofibers (ii). b) Topography map (i) and short-circuit current map of I3D2 nanofibers (ii). Conductivity curves for AVI3D2 at point 1 (c) and point 2 (d), demonstrating conductive nature of the AVI3D2 nanofibers. Scale bar on all images is 5 μm.

and AVI3D2 were studied in solution at 8 mM (pH 4 and pH 8) through Electron Spin Resonance (ESR) Spectroscopy coupled with UV excitation. At pH 8, a characteristic viologen radical cation signature ($g = 2.0033 \pm 0.0002$) was evident after ≈1 hour of excitation, which was found to be stable in air and saturate over time (Figures 4a, S22 and S24).[32] However, at pH 4 AV demonstrated diamagnetic behavior (Figure S23), which has been witnessed previously for methyl-viologen derivatives on account of radical cation induced dimerization and the opposing electron spin states in the diradical.[32] Therefore, a similar configuration for AV can be suggested, as the diradical cation forms, it will likely be stabilized by intermolecular interactions between the viologen units observed in the NOESY studies. AVI3D2 has a weak radical signal at pH 4, where it is known to be in a β-sheet conformation and has intermolecular interactions between the aryl-viologen units (Figures 4b and S25). Unlike a diradical configuration where the radicals are paired, the β-sheet conformation of AVI3D2 is an extended stack, which may generate a confined electronic environment with a slight twist and/or it may contain an odd number of unpaired radicals. Importantly, these ESR studies demonstrate that the aryl-viologen units can be easily reduced through electron donation from the D-A pair and provides further evidence of a confined electronic environment induced by the β-sheet self-assembly of AVI3D2.

When considering this in the context of the conductive nanofibers, a constant stream of electrons, coupled with the D-A

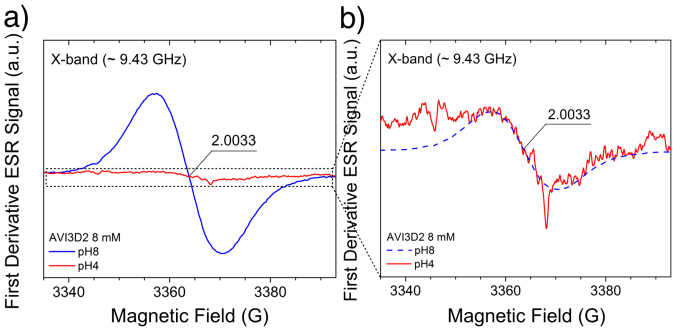

Fig. 4 a) X-band (∼ 9.43 GHz) first derivative ESR spectra of AVI3D2 (8 mM) at pH4 and pH8 following UV irradiation. b) Magnification of AVI3D2 (8 mM) at pH4 coupled with a rescaled overlay of AVI3D2 at pH8 (dashed blue line). The signal at $g = 2.0033 \pm 0.0002$ originates from the viologen radical cation.

pair, will promote the reduction of the dication to either a radical cation or a neutral species. This will produce a mixed valency/redox distribution throughout the assembly. In a solid state, mixed-valency viologen systems are known to have high conductivity due to an electron hopping mechanism from viologen to viologen in different redox states.[15,33] Our spectroscopic and ESR studies suggest that the directionality of the β-sheet interactions drive the AV moieties into close proximity. Therefore, we can hypothesize a mechanism based on a confined electronic environment, where electron transfer (hopping) from viologen to viologen is enhanced along the nanofiber's supramolecular stack. Similarly, previous studies of nanofibrillar structures demonstrated that π-π stacking of conductive molecules can facilitate charge separation and allow for electron and hole transport through intermolecular π-electron delocalization.[2,3]

The directional organization present in the assembled AVI3D2 nanofibers is likely to produce a variation in charge carrier mobility along the different axes of the nanofibers. As previously mentioned, the thicker fibers/denser regions appear to have an increased conductivity, for example at -10 V point 2 is seven times larger than point 1 (Figures 3c and 3d). This could be a product of fiber orientation and charge carrier mobility, although this is difficult to determine from the AFM topography maps. It is also difficult to deduce the quality and orientation of contact between the fibers and substrate. With c-AFM being a contact-based measurement, differences in contact are likely to generate variations in the conductivity curve measurements.

We report an AV labelled pentapeptide sequence, which can form conductive nanofibers through pH triggered β-sheet assembly. To explore the relationship between the secondary structure and the conductive properties of the nanofibers, we utilized spectroscopic techniques, which verified the β-sheet structure. PL quenching through PET, NOESY 2D-NMR and different degrees of red-shift in the CD spectra suggested that the AV portion of the molecules are in close contact, generating a less twisted parallel β-sheet. c-AFM identified the semi-conductive behavior of the nanofibers, which had an enhanced conductivity when compared to amorphous aggregates. We propose that the high conductivity of these nanofibers is a product of a mechanism involving the reduction of the viologen portion of the molecule, followed by electron transport (hopping) between viologens along the supramolecular stack. These conductive nanofibers, with facile and controllable assembly in aqueous environments have potential for future exploration in optoelectronic applications.

Conflicts of interest

There are no conflicts to declare.

Acknowledgments

The authors thank the ERC ('ASPiRe', 240629) and Marie Curie (FP7 'SASSYPOL' ITN, 607602) for funding. We also thank the EPSRC Cambridge NanoDTC (EP/G037221/1) for access to their AFM equipment.

Notes and references

1 L. Pospisil, M. Hromadova, N. Fanelli, M. Valasek, V. Kolivoska and M. Gal, *Phys. Chem. Chem. Phys.*, 2011, **13**, 4365–4371.
2 L. Zang, *Acc. Chem. Res.*, 2015, **48**, 2705–2714.
3 J. W. Chung, H. Yang, B. Singh, H. Moon, B.-k. An, S. Y. Lee and S. Y. Park, *J. Mater. Chem.*, 2009, **19**, 5920–5925.
4 K. Tao, P. Makam, R. Aizen and E. Gazit, *Science*, 2017, **358**, eaam9756.
5 S. Fleming and R. V. Ulijn, *Chem. Soc. Rev.*, 2014, **43**, 8150–8177.
6 C. G. Pappas, R. Shafi, I. R. Sasselli, H. Siccardi, T. Wang, V. Narang, R. Abzalimov, N. Wijerathne and R. V. Ulijn, *Nat. Nanotechnol.*, 2016, **11**, 960–967.
7 P. W. J. M. Frederix, G. G. Scott, Y. M. Abul-Haija, D. Kalafatovic, C. G. Pappas, N. Javid, N. T. Hunt, R. V. Ulijn and T. Tuttle, *Nat. Chem.*, 2014, **7**, 30–37.
8 C. Guo, Y. Luo, R. Zhou and G. Wei, *Nanoscale*, 2014, **6**, 2800–2811.
9 M. Reches and E. Gazit, *Nano Lett.*, 2004, **4**, 581–585.
10 M. Reches and E. Gazit, *Science*, 2003, **300**, 625–627.
11 A. Lakshmanan, D. W. Cheong, A. Accardo, E. Di Fabrizio, C. Riekel and C. A. E. Hauser, *Proc. Natl. Acad. Sci.*, 2013, **110**, 519–524.
12 G. L. Eakins, J. K. Gallaher, R. A. Keyzers, A. Falber, J. E. A. Webb, A. Laos, Y. Tidhar, H. Weissman, B. Rybtchinski, P. Thordarson and J. M. Hodgkiss, *J. Phys. Chem. B*, 2014, **118**, 8642–8651.
13 G. L. Eakins, R. Pandey, J. P. Wojciechowski, H. Y. Zheng, J. E. A. Webb, C. Valéry, P. Thordarson, N. O. V. Plank, J. A. Gerrard and J. M. Hodgkiss, *Adv. Funct. Mater.*, 2015, **25**, 5640–5649.
14 J. S. Lee, I. Yoon, J. Kim, H. Ihee, B. Kim and C. B. Park, *Angew. Chem. Int. Ed.*, 2011, **50**, 1164–1167.
15 W. W. Porter and T. P. Vaid, *J. Org. Chem.*, 2005, **70**, 5028–5035.
16 W. Zhang, S. Gan, A. Vezzoli, R. J. Davidson, D. C. Milan, K. V. Luzyanin, S. J. Higgins, R. J. Nichols, A. Beeby, P. J. Low, B. Li and L. Niu, *ACS Nano*, 2016, **10**, 5212–5220.
17 X. Liu, K. G. Neoh and E. T. Kang, *Langmuir*, 2002, **18**, 9041–9047.
18 T. Janoschka, S. Morgenstern, H. Hiller, C. Friebe, K. Wolkersdorfer, B. Haupler, M. D. Hager and U. S. Schubert, *Polym. Chem.*, 2015, **6**, 7801–7811.
19 G. Wu, M. Olesińska, Y. Wu, D. Matak-Vinkovic and O. A. Scherman, *J. Am. Chem. Soc.*, 2017, **139**, 3202–3208.
20 D. E. Clarke, C. D. J. Parmenter and O. A. Scherman, *Angew. Chem. Int. Ed.*, 2018, **57**, 7709–7713.
21 J. Peon, X. Tan, J. D. Hoerner, C. Xia, Y. F. Luk and B. Kohler, *J. Phys. Chem. A*, 2001, **105**, 5768–5777.
22 B. Valeur and M. N. Berberan-Santos, *Molecular Fluorescence: Principles and Applications, Second Edition*, Wiley-VCH Verlag GmbH & Co. KGaA, 2012.
23 S. Doose, H. Neuweiler and M. Sauer, *ChemPhysChem*, 2009, **10**, 1389–1398.
24 R. M. Young, S. M. Dyar, J. C. Barnes, M. Juríček, J. F. Stoddart, D. T. Co and M. R. Wasielewski, *J. Phys. Chem. A*, 2013, **117**, 12438–12448.
25 S. M. Dyar, J. C. Barnes, M. Juríček, J. F. Stoddart, D. T. Co, R. M. Young and M. R. Wasielewski, *Angew. Chem. Int. Ed.*, 2014, **53**, 5371–5375.
26 M. C. Manning, M. Illangasekare and R. W Woody, *Biophys. Chem.*, 1988, **31**, 77–86.
27 C. L. Nesloney and J. W. Kelly, *Bioorg. Med. Chem.*, 1996, **4**, 739–766.
28 E. T. Pashuck, H. Cui and S. I. Stupp, *J. Am. Chem. Soc.*, 2010, **132**, 6041–6046.
29 J. Kubelka and T. A. Keiderling, *J. Am. Chem. Soc.*, 2001, **123**, 12048–12058.
30 A. Lampel, S. A. McPhee, H.-A. Park, G. G. Scott, S. Humagain, D. R. Hekstra, B. Yoo, P. W. J. M. Frederix, T.-D. Li, R. R. Abzalimov, S. G. Greenbaum, T. Tuttle, C. Hu, C. J. Bettinger and R. V. Ulijn, *Science*, 2017, **356**, 1064–1068.
31 P. M. S. Monk, D. R. Rosseinsky and R. J. Mortimer, in *Electrochromic materials and devices based on viologens*, Wiley-VCH, 2013, pp. 57–90.
32 A. T. Buck, J. T. Paletta, S. A. Khindurangala, C. L. Beck and A. H. Winter, *J. Am. Chem. Soc.*, 2013, **135**, 10594–10597.
33 S. V. Rosokha and J. K. Kochi, *Acc. Chem. Res.*, 2008, **41**, 641–653.